This is the peer reviewed version of the following article:[Bastos G, Franco E. Dynamic tube model predictive control for a class of soft manipulators with fluidic actuation. Int J Robust Nonlinear Control. 2023;1-20], which has been published in final form at [https://doi.org/10.1002/rnc.6598]. This article may be used for non-commercial purposes in accordance with Wiley Terms and Conditions for Use of Self-Archived Versions. This article may not be enhanced, enriched or otherwise transformed into a derivative work, without express permission from Wiley or by statutory rights under applicable legislation. Copyright notices must not be removed, obscured or modified. The article must be linked to Wiley's version of record on Wiley Online Library and any embedding, framing or otherwise making available the article or pages thereof by third parties from platforms, services and websites other than Wiley Online Library must be prohibited.

ORIGINAL ARTICLE

Journal Section

Dynamic tube-MPC for a class of soft continuum manipulators with fluidic actuation

Guaraci Bastos Jr.[1*] | **Enrico Franco**[2*]

Controlling soft continuum manipulators is a challenging task due to the structural compliance of these systems which results in underactuation. While a variety of control approaches have been proposed for regulation tasks, tracking control requires further investigation. To this end, a new dynamic tube-Model Predictive Control formulation is presented, which includes an ancillary control law constructed analytically with an energy-shaping approach. Two different models are considered: *i*) a rigid-link model with direct-torque actuation, which is representative of miniature soft continuum manipulators supplied by digital pressure regulators; *ii*) an extended model that includes the pressure dynamics of the fluid, which is representative of fluidic actuation by means of a variable flow rate. The effectiveness of the proposed algorithm is demonstrated with numerical simulations considering bounded external disturbances, either constant or time-varying.

KEYWORDS

dynamic tube-MPC, bounded disturbances, unmatched disturbances, underactuated systems, soft continuum manipulators, trajectory tracking

[1]Mechanical Engineering Department, Federal University of Pernambuco, Recife-PE, Brazil

[2]Mechatronics in Medicine Laboratory, Mechanical Engineering Department, Imperial College London, UK

Correspondence
G. Bastos Jr., Mechanical Engineering Department, Federal University of Pernambuco, Av. Prof. Moraes Rego 1235, Recife-PE 50670-901, Brazil
Email: guarajr.bastos@gmail.com

Funding information
UK Engineering and Physical Sciences Research Council, grant EP/R511547/1 and EP/W004224/1.

Abbreviations: MPC, Model Predictive Control; IDA-PBC, Interconnection and damping assignment passivity based control; DOFs, degrees of freedom.

[*]Equally contributing authors.

1 | INTRODUCTION

Soft continuum manipulators are a special class of soft robots characterized by serial strucure, high compliance, light weight, and affordable cost compared to conventional rigid manipulators. The majority of soft continuum manipulators have been developed at miniature scale, such as the flexible micro actuator [1] and subsequent designs [2]. Typical applications include inspection [3] and minimally invasive surgery [4, 5]. More recently, larger soft continuum manipulators have been investigated as part of anthropomorphic robots [6]. While all the above systems employ pneumatic actuation, other continuum manipulators employ cable actuation, which is characterized by a different dynamics and by specific challenges (i.e., friction of the cables) [7, 8, 9, 10]. Controlling soft continuum manipulators is a challenging problem since their high compliance results in underactuation [11]. In practice, satisfactory performance can be achieved with kinematic-based controllers, provided that a fast response is not required [12]. High responsiveness can be achieved by employing high-gain controllers, such as sliding mode control (SMC) [13], which however comes at the cost of increasing the stiffness of the system in closed-loop [14]. A promising approach to modeling and control of soft continuum manipulators involves the use of the port-Hamiltonian formulation and of passivity-based-control methodologies [15]. In particular, the *Interconnection-and-damping-assignment passivity-based-control* methodology (IDA-PBC) [16] provides compelling advantages, including a physical interpretation of the control action in terms of mechanical energy of the system, and the use of small gains which preserve closed-loop compliance. As a result, IDA-PBC designs for soft continuum manipulators can yield a smoother transient and a reduced control action compared to high-gain approaches [11]. However, IDA-PBC is specific to regulation tasks, and it has only been extended to tracking for some classes of systems. A further challenge associated to soft continuum manipulators, is the presence of disturbances and model uncertainties, which are ubiquitous in engineering practice. These effects have been accounted for in the literature by introducing in the control law either an adaptive observer [17] or an integral action [18]. Finally, the use of fluidic actuation, either pneumatic or hydraulic, introduces further control-related challenges, since the control action is mediated by the dynamics of the pressurized fluid. To overcome this complication, extended dynamical models and corresponding model-based controllers have recently been investigated [19, 20, 21].

Most literature on the control of soft continuum manipulators, including IDA-PBC designs, has been focused on regulation tasks. An extension of IDA-PBC for tracking tasks was proposed in [22], however it only applies to mechanical systems with constant inertia matrix, thus it is not well suited to soft continuum manipulators. Notable results on tracking control of soft manipulators have employed SMC algorithms [13], which however require high gains. Data-driven approaches that employ machine learning techniques, such as recurrent deep neural networks, have been employed with good results for tracking control of mobile robots [23]. However, employing these strategies for soft manipulators is problematic due to the limited durability of these systems compared to their rigid counterparts, which makes it impractical to collect large datasets. Conversely, model predictive control (MPC) has proved effective for the tracking control of soft continuum manipulators without disturbances and considering a smooth trajectory (see [6] for details). MPC is a feedback control strategy that requires solving an optimal control problem at each iteration [24, 25, 26, 27], it allows accounting for state and/or control constraints, and it is ideally suited for trajectory tracking. Robust MPC implementations can account for external disturbances and for state/input constraints [28]. Tube-MPC is another robust approach that can also account for model/plant discrepancies by employing an ancillary control action alongside MPC. In [29] the ancillary control was computed using MPC and the resulting algorithm was employed for nonlinear systems. Subsequent tube-MPC algorithms have demonstrated further advantages, such as generality and suitability to software implementation [30, 31, 32]. Tube-MPC algorithms have also been employed for linear systems with additive disturbances in [33], have been investigated for uncertain multiagent systems in [34], and for the tracking control of spacecrafts with external disturbances in [35]. Dynamic tube-MPC promises further performance

and robustness enhancements compared to tube-MPC thanks to its added flexibility, which results from treating the tube geometry as a design variable to be optimized [36]. In particular, the dynamic tube-MPC implementation [36] is intended for fully actuated system, and it involves computing the ancillary control action and the tube dynamics analytically, based on sliding-mode principles. In our previous work [37], we have proposed a dynamic tube-MPC algorithm for underactuated mechanical systems by combining the MPC formulation with an ancillary control action and a tube dynamics derived analytically using energy-shaping principle with the IDA-PBC methodology. In spite of its potential advantages, to the best of our knowledge, dynamic tube-MPC has not yet been formalized for soft continuum manipulators. The main technical challenges in this respect include the underactuated nature of this type of systems, the possible lack of full state feedback, the presence of disturbances and model uncertainties, and the complex dynamics of the system, which includes the dynamics of the pressurized fluid in case of fluidic actuation. The latter point results in a dynamical model that is not in affine form, thus employing the approach proposed in [37] could result in degraded performance.

This work investigates the trajectory tracking problem for a class of soft continuum inextensible manipulators with fluidic actuation that bend on a plane due to pressurization of one or more internal chambers. To this end, a dynamic tube-MPC is proposed for soft continuum planar manipulators with either direct-torque actuation achieved through a regulated pressure source, or with fluidic actuation by means of a variable flow rate. In summary, the main contributions of this work include the following points.

- A new dynamic tube-MPC implementation for underactuated systems is proposed which, differently from [37], employs time-varying tube parameters and corresponding constraints hence it is more general.
- The ancillary control and the tube dynamics are formulated with the IDA-PBC methodology for a class of planar soft continuum inextensible manipulators with bounded disturbances. Both direct-torque actuation through a regulated pressure and fluidic actuation through a variable flow rate are considered. Convergence conditions are discussed with a Lyapunov approach in relation to the tuning parameters.
- Simulation results are presented for both direct-torque actuation and fluidic actuation by considering different trajectories and time-varying as well as constant external disturbances, either matched or unmatched. The proposed algorithm is compared with alternative tube-MPC implementations demonstrating improved performance.

The rest of the paper is organized as follows. Section 2 summarizes the dynamic tube-MPC algorithm outlining its principle and key components. Section 3 details the ancillary control and the tube dynamics for soft continuum manipulators. Section 4 presents the simulation results, while Section 5 contains concluding remarks.

2 | DYNAMIC TUBE-MPC FOR UNDERACTUATED MECHANICAL SYSTEMS

2.1 | Overview of dynamic tube-MPC

The principle of dynamic-tube MPC [36], which inspired our previous work [37], is outlined here for completeness. This approach is intended for fully actuated systems and defines the control policy π as the sum of the control input u, which is computed with an MPC implementation that has additional constraints related to the dynamic tube variables to be optimized (i.e. α is part of the set of design variables), and the ancillary control input u_{smc}, which is an SMC controller consisting of a continuous term and a switching term. In [36] the optimization problem is formulated for

the fully actuated system dynamics in the so-called affine form

$$\dot{x} = f(x) + u - \delta,$$

where δ is a bounded disturbance, that is $|\delta| < \varepsilon$. The dynamic tube-MPC control law is thus

$$\begin{aligned} \pi &= u + u_{\text{smc}}, \\ \min(J)_{u,v} &= h(\check{x}(t_f)) + \int_{t_i}^{t_f} l(\check{x}, u, u_{\text{smc}}, \alpha, v)\, d\tau, \\ u_{\text{smc}} &= -f(x) - k_1 s - k_2 \text{sign}(s/\phi), \\ \dot{\phi} &= \varepsilon - \alpha\phi, \end{aligned}$$

where $s = \dot{x}_d - \dot{x} - \lambda(x_d - x)$ and $s = 0$ is the sliding surface, x_d is the desired trajectory, and ϕ is the dynamic tube. The terms k_1, k_2 are tuning parameters of the SMC, and the MPC optimization is subject to the constraints

$$\begin{aligned} \dot{\check{x}} &= f(\check{x}) + u, \\ \dot{\phi} &= \varepsilon - \alpha\phi, \\ \dot{\alpha} &= v, \end{aligned}$$

in addition to the initial conditions and the final conditions. In particular, the tube geometry depends on the design variable α and on the tube dynamics $\dot{\phi}$ which is computed analytically.

The dynamic tube-MPC has been extended in [37] to underactuated mechanical systems in affine form by computing the ancillary control law with the IDA-PBC methodology [16] instead of using SMC principles. The system dynamics for underactuated mechanical systems can be expressed in port-Hamiltonian form by defining the total energy as

$$H(q,p) = \frac{1}{2} p^T M^{-1} p + \Gamma,$$

sum of the kinetic energy and the potential energy Γ. The system states are the position $q \in \mathbb{R}^n$ and the momenta $p = M\dot{q} \in \mathbb{R}^n$, where $M = M^T > 0$ is the inertia matrix. The open-loop dynamics in the presence of a physical damping matrix $D = D^T > 0$ and of the matched disturbances δ (i.e. only affecting the actuated states) is then

$$\begin{bmatrix} \dot{q} \\ \dot{p} \end{bmatrix} = \begin{bmatrix} 0 & I \\ -I & -D \end{bmatrix} \begin{bmatrix} \nabla_q H \\ \nabla_p H \end{bmatrix} + \begin{bmatrix} 0 \\ G(u - \delta) \end{bmatrix}. \tag{1}$$

The input matrix is $G \in \mathbb{R}^{n \times m}$, with $\text{rank}(G) = m < n$, and the control input is $u \in \mathbb{R}^m$. The term $\nabla_q H$ is the vector of partial derivatives in q, and $\nabla_p H$ is the vector of partial derivatives in p. The IDA-PBC control law is constructed to achieve the closed-loop dynamics

$$\begin{bmatrix} \dot{q} \\ \dot{p} \end{bmatrix} = \begin{bmatrix} 0 & M^{-1} M_d \\ -M_d M^{-1} & J_2 - D_d \end{bmatrix} \begin{bmatrix} \nabla_q H \\ \nabla_p H \end{bmatrix} - \begin{bmatrix} 0 \\ G\delta \end{bmatrix}. \tag{2}$$

where $H_d = \frac{1}{2} p^T M_d^{-1} p + \Gamma_d$ is the desired Hamiltonian, and Γ_d is chosen so that it has a strict minimizer in q^*, that is

$q^* = \text{argmin}\,(\Gamma_d)$. The closed-loop damping in (2) is defined as $D_d = (Gk_vG^T + DM^{-1}M_d)$, with $M_d = M_d^T > 0$ the closed-loop inertia matrix and $k_v = k_v^T > 0$ a constant gain matrix, while $J_2 = -J_2^T$ is a free-parameter matrix. The IDA-PBC control law that achieves the desired closed-loop dynamics (2) is [16]

$$u_{\text{es}} = G^{\dagger}\left(\nabla_q H - M_d M^{-1}\nabla_q H_d + J_2 M_d^{-1} p\right) - k_v G^T \nabla_p H_d, \tag{3}$$

where $G^{\dagger} = \left(G^T G\right)^{-1} G^T$. The terms M_d and Γ_d should satisfy the partial-differential-equations (PDEs) $\forall\,(q,p) \in \mathbb{R}^{2n}$

$$G^{\perp}\left(\nabla_q (p^T M^{-1} p) - M_d M^{-1}\nabla_q (p^T M_d^{-1} p) + 2J_2 M_d^{-1} p\right) = 0,$$
$$G^{\perp}\left(\nabla_q \Gamma - M_d M^{-1}\nabla_q \Gamma_d\right) = 0,$$

where $G^{\perp}$ is such that $G^{\perp}G = 0$ and $\text{rank}\,(G^{\perp}) = n-m$. The dynamic-tube MPC for underactuated mechanical systems [37] consists thus in defining the control policy π as the sum of the MPC control action u, which considers additional constraints related to the dynamic tube variables (i.e. the parameter α), and the ancillary control action

$$u_{\text{ida-pbc}} = \begin{cases} u_{\text{es}} & H_d\,(q,p) < c, \\ u_{\text{es}} + u_0 & H_d\,(q,p) \geq c, \end{cases} \tag{4}$$

where u_{es} is given in (3). The parameter c representing the width of the dynamic tube, and the term u_0 are defined as

$$\begin{aligned} u_0 &= -\alpha c\left(G^T \nabla_p H_d\right), \\ \dot{c} &= \left|\nabla_p H_d^T G\right|\varepsilon - \alpha\left(\nabla_p H_d^T G G^T \nabla_p H_d\right) c, \end{aligned} \tag{5}$$

where α is a design variable computed by the MPC optimization problem, while ε is the disturbance bound, that is $|\delta| < \varepsilon$. It follows from *Proposition 1* in [37] that (4) and (5) ensure that all system trajectories starting outside $\Omega_c = \left\{(q,p) \in \mathbb{R}^{2n} | H_d\,(q,p) < c\right\}$ converge to Ω_c asymptotically, and all system trajectories originating in Ω_c remain in Ω_c indefinitely provided that $D_d > 0, k_v \geq \alpha c$, and that $q^* = \text{argmin}(\Gamma_d)$. In practice, the feedback control law corresponding to the dynamic tube-MPC [37] is activated when the output error is larger than a predefined tolerance. Conversely, the control input corresponds to a feedforward control action u_{ff} computed as a stable inversion dynamics problem with an optimal control approach as in [38], which is outlined in the next subsection.

2.2 | Overview of feedforward control

The feedforward control action u_{ff} is computed by solving an inverse dynamics problem related to a desired trajectory $y_d(t)$ for the system's output $y(t) = h(q(t))$. This is an open-loop control problem used as reference when the output error is smaller than a predefined tolerance. The equations of motion for mechanical systems expressed using Newton's second law are

$$M(q)\ddot{q}(t) + g(q(t), \dot{q}(t), t) = Gu(t),$$

where q is the vector of generalized coordinates in position, $M(q) > 0$ is the inertia matrix, and $g(q, \dot{q}, t)$ is the vector of internal and complementary inertia forces. Differential flatness is a powerful concept for the study of inverse

dynamics problems: a flat system is one where states and control input can be determined in a purely algebraic fashion from the flat outputs and their derivatives. In linear systems, controlability and flatness properties are equivalent concepts. Thus, considering the output $y = G^T q$ and its desired trajectory, the inverse dynamics of the linearized system is

$$u_{\text{ff}}(t) = G^{-1}(MG\ddot{y}_d(t) + CG\dot{y}_d(t) + Ky_d(t)),$$

which is expressed as a function of the output and its derivatives by imposing $y(t) = y_d(t)$.

Unfortunately, underactuated systems are often characterized by an unstable internal dynamics related to the unactuated states. Thus, stable inverse methods, such as those based on optimal control theory, are required to compute the feedforward action. Defining for illustrative purposes the performance index

$$J = \int_{t_0}^{t_f - dt} ((y_d(t) - y(t))^2 + u_{\text{ff}}(t)^2)\, dt + (y_d(t_f) - y(t_f))^2,$$

a dynamic programming problem can be formulated, which employs a backward iteration starting with $J(t_f) = (y_d(t_f) - y(t_f))^2$. This approach relies on the fact that a sub-arc of an optimal control trajectory is also an optimal sub-arc. Considering the system dynamics expressed in general form

$$\dot{\mathbf{x}}(t) = \mathbf{f}(\mathbf{x}(t), u(t), t), \quad \mathbf{x}(0) = \mathbf{x}_0$$

where $\mathbf{x} = [q\ \dot{q}]^T$, the discretized performance index at the following steps $i = N_{\text{tot}} - 1, N_{\text{tot}} - 2, \ldots, 1$ is thus

$$J^{(i)} = \min_{u_{\text{ff}}^{(i)}} \left([(y_d(t_i) - y^{(i)})^2 + (u_{\text{ff}}^{(i)})^2]dt + J^{(i+1)}(\mathbf{x}^{(i)} + \mathbf{f}(\mathbf{x}^{(i)}, u_{\text{ff}}^{(i)})dt \right).$$

The feedforward control u_{ff} is then computed by solving the optimization problem

$$u_{\text{ff}}^{*(i)} = \arg \min_{u_{\text{ff}}^{(i)}} \left([(y_d(t_i) - y^{(i)})^2 + (u_{\text{ff}}^{(i)})^2]dt + J^{(i+1)}(\mathbf{x}^{(i)} + \mathbf{f}(\mathbf{x}^{(i)}, u_{\text{ff}}^{(i)})dt \right).$$

Since the analytical solution of the above problem can be challenging in general, a direct transcription method [38] which follows the rule *first discretize, then optimize* is employed in this work. Alternative approaches for solving the inverse dynamics of underactuated systems include direct multiple shooting methods, such as [39].

2.3 | Dynamic tube-MPC implementation

The dynamic tube-MPC for underactuated mechanical systems [37] is constructed by including the ancillary control (4) and the dynamic tube equation (5) as equality constraints. In particular, the variables related to the dynamic tube α, $\dot{\alpha}$, $\ddot{\alpha}$, c, $\dot{c}$, $\ddot{c}$ and u_{aux}, which acts as an auxiliary control variable, are included in the set of design variables at each time step i (together with the pressure P and its time-derivative $\dot{P}$ in case of fluidic actuation) thus

$$\chi^{(i)} = \left(q^{(i)},\ \dot{q}^{(i)},\ \ddot{q}^{(i)},\ a^{(i)}, P^{(i)},\ \dot{P}^{(i)},\ c^{(i)},\ \alpha^{(i)},\ \dot{c}^{(i)},\ \dot{\alpha}^{(i)},\ \ddot{c}^{(i)},\ \ddot{\alpha}^{(i)},\ u^{(i)},\ u_{\text{aux}}^{(i)} \right)^T,$$

where $i = 1, \ldots, N_{tot}$, and N_{tot} is reduced at each iteration in a receding-horizon optimization problem according to MPC principles. The total set of design variables is $\chi = (\chi^{(1)} \;\; \chi^{(2)} \;\; \ldots \;\; \chi^{(N_{tot})})^T$ and has dimension $(N_{\text{tot}})(4n+4m+6)$. The variables $c, \dot{c}, \ddot{c}$ are not independent but are computed analytically with (5) thus they could be eliminated in theory. However, our experience indicates that keeping these variables allows improving convergence due to better numerical conditioning for the tracking problem (i.e. systems and trajectories) considered here. Differently from the dynamic tube-MPC algorithm [37], we account for an independent tube variable α with a non-constant time derivative $\dot{\alpha}$ by employing a new equality constraint $\mathbf{c}_\alpha$ thus resulting in a more general implementation. The resulting nonlinear programming problem is thus

$$
\begin{aligned}
\mathcal{P}: \min_{\chi} \quad & J = \int_{t_k}^{t_f} (\gamma_{\text{obj}}(\alpha(t))^2 + \beta_{\text{obj}} u(t)^2)\, dt \\
\text{s.t.} \quad & \mathbf{c}_{\text{mot}}(\chi) = \mathbf{res}(q, \dot{q}, \ddot{q}, P, \dot{P}, u) \\
& \mathbf{c}_{\text{tube}}(\chi) = -\dot{c}(t) + \varepsilon w_1(q, \dot{q}) - c(t)\alpha(t) w_2(q, \dot{q}, P) \\
& \mathbf{c}_{\text{aux}}(\chi) = -(u_{\text{aux}} + u) + u_{\text{ida-pbc}}(q, \dot{q}, P) \\
& \mathbf{c}_{\alpha}(\chi) = -\alpha(t+dt) + \alpha(t) + \dot{\alpha}(t+dt)dt + (\ddot{\alpha}(t+dt) + \ddot{\alpha}(t))dt^2/4 \\
& \mathbf{A}_{\text{intg}}\chi - \mathbf{b}_{\text{intg}} = 0 \\
& 0 = -q(t_k) + q_{\text{out}} \\
& 0 = -y(t_f) + y_d(t_f) \\
& \mathbf{v}^{c}_{\text{ineq}}(\chi) \triangleq c(t) > 0 \\
& \mathbf{v}^{\alpha}_{\text{ineq}}(\chi) \triangleq \alpha(t) > 0
\end{aligned}
$$

where γ_{obj} and β_{obj} are weights of the elements of J. The term $\mathbf{res}(q, \dot{q}, \ddot{q}, P, \dot{P}, u)$ is the residual of the dynamic equation considering the control input u, and $\mathbf{c}_{\text{mot}} \approx 0$ when a solution of this equation is found. The constraint $\mathbf{c}_{\text{tube}}$ represents the dynamic tube equation, the constraint $\mathbf{c}_{\text{aux}}$ is related to the ancillary control $u_{\text{ida-pbc}}(q, \dot{q}, P)$, and the constraint $\mathbf{c}_\alpha$ accounts for the fact that both α and $\dot{\alpha}$ are time-varying. Thus, differently from [37], accounting for $\ddot{c}$ and $\ddot{\alpha}$ results in a larger nonlinear programming problem (NLP), that is a larger search domain for the design variables, which is beneficial for finding optimal solutions to more complex tracking problems. However, the gradient-based

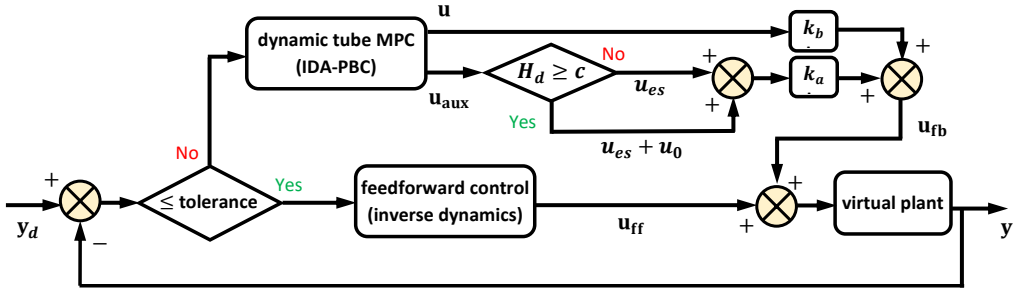


FIGURE 1 Block diagram of the dynamic tube-MPC algorithm for underactuated mechanical systems.

search algorithm employed for the NLP yields additional locally optimal solutions, which should be assessed with respect to the tracking tasks (i.e., confirming that the system follows the prescribed trajectory).

The matrix $\mathbf{A}_{\text{intg}}$ and the vector $\mathbf{b}_{\text{intg}}$ result from the time integration with the generalized$-\alpha$ method [40], which yields a stable convergence for constrained mechanical systems [41], hence it is well suited for trajectory tracking. The generalized-α method is a generalization of the Newmark formula [42], and it can be written as

$$\dot{q}(t+dt) = \dot{q}(t) + (1-\gamma)a(t)dt + \gamma a(t+dt)dt \tag{6}$$

$$q(t+dt) = q(t) + \dot{q}(t)dt + \left(\frac{1}{2}-\beta\right)a(t)dt^2 + \beta a(t+dt)dt^2 \tag{7}$$

$$a(t+dt) = \frac{-\alpha_m a(t) + (1-\alpha_f)\ddot{q}(t+dt) + \alpha_f \ddot{q}(t)}{(1-\alpha_m)} \tag{8}$$

where $\alpha_m = \frac{2\rho_\infty - 1}{\rho_\infty + 1}$, $\alpha_f = \frac{\rho_\infty}{\rho_\infty + 1}$, $\gamma = \frac{1}{2} - \alpha_m + \alpha_f$, $\beta = \frac{1}{4}(\gamma + \frac{1}{2})^2$ are numerical parameters that can be freely chosen to combine unconditional stability and second-order accuracy, and $a(t)$ is the so-called pseudo acceleration. The parameters $\alpha_m, \alpha_f, \gamma, \beta$ depend on the spectral radius at infinite frequencies $\rho_\infty \in [0,1]$, thus varying ρ_∞ from 1 to 0 allows increasing the numerical damping [40]. Note that these equation have a linear structure with respect to the design variables, thus their differentiation leads to constant matrices which depend on the numerical parameters of the generalized-α method, that is

$$\mathbf{A}_k^\alpha = \begin{pmatrix} 0 & -I & 0 & -(1-\gamma)Idt & 0 \\ -I & -Idt & 0 & -(\frac{1}{2}-\beta)Idt^2 & 0 \\ 0 & 0 & -\alpha_f I & \alpha_m I & 0 \end{pmatrix},$$

and

$$\mathbf{A}_{k+1}^\alpha = \begin{pmatrix} 0 & I & 0 & -\gamma Idt & 0 \\ I & 0 & 0 & -\beta Idt^2 & 0 \\ 0 & 0 & -(1-\alpha_f)I & (1-\alpha_m)I & 0 \end{pmatrix}.$$

The Jacobian matrix can be computed as

$$\mathbf{A}_{\text{intg}} = \left(\begin{array}{c|c|c|c|c|c} \mathbf{A}_k^\alpha & \mathbf{A}_{k+1}^\alpha & & & & \\ \hline & \mathbf{A}_k^\alpha & \mathbf{A}_{k+1}^\alpha & & & \\ \hline & & & \ddots & & \\ \hline & & & & \mathbf{A}_k^\alpha & \mathbf{A}_{k+1}^\alpha \end{array}\right),$$

which has a block diagonal structure, while $\mathbf{b}_{\text{intg}} = 0$. In addition, boundary conditions are established for q at the beginning and for y at the end of the time horizon. The complete set of equality constraints is thus given by $\mathbf{c}_{\text{eq}} = (\mathbf{c}_{\text{mot}}^{(1)}, \mathbf{c}_{\text{tube}}^{(1)}, \mathbf{c}_{\text{aux}}^{(1)}, \mathbf{c}_{\alpha}^{(1)} \ldots, \mathbf{c}_{\text{mot}}^{(N_{\text{tot}})}, \mathbf{c}_{\text{tube}}^{(N_{\text{tot}})}, \mathbf{c}_{\text{aux}}^{(N_{\text{tot}})}, \mathbf{c}_{\alpha}^{(N_{\text{tot}})})$, and the set of inequality constraints is given by $\mathbf{v}_{\text{ineq}} = (\mathbf{v}_{\text{ineq}}^{\alpha\ (1)}, \mathbf{v}_{\text{ineq}}^{c\ (1)}, \ldots, \mathbf{v}_{\text{ineq}}^{\alpha\ (N_{\text{tot}})}, \mathbf{v}_{\text{ineq}}^{c\ (N_{\text{tot}})})$, where $\mathbf{v}_{\text{ineq}}^{\alpha}$ and $\mathbf{v}_{\text{ineq}}^{c}$ impose positive values for α and c. In particular, minimizing the tube variable α is equivalent to minimizing the output error in the objective function of the dynamic tube-MPC implementation.

In summary, the feedforward control is computed as a stable inversion dynamics problem with an optimal control approach as in [38], and the feedback control law is activated and computed according to $\mathcal{P}$ when the output error is

larger than a predefined tolerance (see Figure 1, where $H_d(q, \dot{q})$ is the mechanical energy of the closed-loop system). Compared to the IDA-PBC control (3), the ancillary control includes an additional dissipative term $u_0(q, \dot{q})$, which is accounted for in the optimization problem. Thus, the tracking error is minimized indirectly in the performance index, and additional equality constraints based on the tube dynamics (5) are introduced in the MPC optimization problem. The resulting dynamic tube-MPC control policy is

$$\pi = u_{\text{fb}} = k_b u + k_a u_{\text{aux}}, \tag{9}$$

where the gains k_b and k_a affect the responsiveness of the system and should be chosen appropriately to achieve a satisfactory performance.

3 | SOFT CONTINUUM PLANAR MANIPULATORS

The main contribution of this work is the formulation of the dynamic-tube MPC for a class of soft continuum inextensible manipulators with fluidic actuation that bend on a plane due to pressurization of one or more internal chambers, which is achieved either with a regulated pressure or a variable flow rate. In the former case, the ancillary control and the tube dynamics only depend on the outputs $y = \theta$ and $\dot{y} = \dot{\theta}$ rather than on the full state (q, p) which may not be measurable. In the latter case, the control input is not affine in the momenta p thus the design of the ancillary control and the dynamic tube equations need to be modified accordingly. Similarly to [36, 37], the ancillary control is obtained analytically and is accounted for in the optimization, and its role is to ensure that the output θ remains in a robust control-invariant tube around the nominal trajectory.

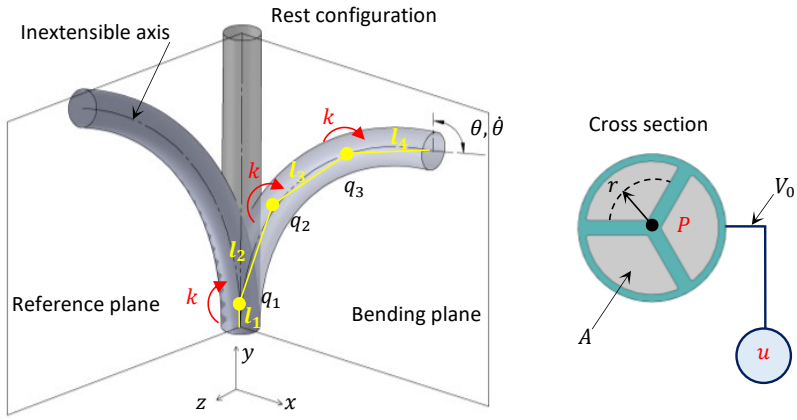


FIGURE 2 Schematic of a soft continuum inextensible manipulator with three equal internal chambers (i.e. one of them being pressurized), and corresponding rigid-link model with $n = 3$. The manipulator always bends on a plane due to pressurization of either one (as shown in the section view) or multiple internal chambers, while extension is prevented by a central intextensible element [11]. The parameters of the rigid links are defined in the Appendix.

3.1 | Dynamical model for direct-torque actuation with regulated pressure

The system dynamics is approximated with a series of rigid-links connected in series by n virtual elastic joints with stiffness k and damping b as in [15, 43, 11] (see Figure 2). This approach is based on the so-called *pseudo rigid body model*, which approximates compliant structures by introducing an arbitrary number of virtual elastic joints (see [44] for details). Since the model has n degrees of freedom (DOFs) and $m = 1$ control input (i.e. in case only one internal chamber is pressurized) it is underactuated. This model is representative of miniature soft continuum manipulators with a uniform cross section actuated by digital pressure regulators [11]. In such case, neglecting the pressure dynamics of the fluid and assuming that the control input corresponds to the bending moment generated by the pressure is a reasonable approximation, provided that the digital pressure regulator is much faster than the soft manipulator itself. The following assumptions are introduced for controller design purposes.

Assumption 1: The tip rotation $\theta = G^T q = \sum_{i=1}^{n} q_i$ and its time derivative $\dot{\theta}$ are known at any instant and are bounded. In addition, all sections of the soft manipulator bend in the same direction, that is $q_i q_j > 0 \; \forall i, j$, however q_i and $\dot{q}_i$ are not directly measurable since they refer to virtual joints.

Assumption 2: The bending stiffness k and the physical damping $D = bI > 0$, where I is the identity matrix of dimensions $n \times n$, are uniform along the length and accurately known. The system moves on an horizontal plane, thus gravity forces are negligible. The disturbances $\delta \in \mathbb{R}^m$ are matched (i.e. they affect the system dynamics in the same way as the control input) and bounded, that is $|\delta| \leq \varepsilon$, where $\varepsilon > 0$ is known.

The Hamiltonian corresponding to the rigid-link model is $H = \frac{1}{2} p^T M^{-1} p + \frac{k}{2} q^T q$. In the absence of disturbances, the energy-shaping control law that achieves the regulation of the tip angle $\theta = \theta^*$ (i.e., $y = y_d$) computed according to the IDA-PBC methodology (3) is

$$u_{\text{es}} = \frac{k}{n}\theta + k_p k_m \left(\theta^* - \theta\right) - \frac{k_v}{k_m}\dot{\theta}, \tag{10}$$

where the tuning parameters are k_m and k_p, which refer to the kinetic energy shaping and to the potential energy shaping respectively, and k_v, which refers to damping assignment [11]. Note that (10) does not depend on the damping b, which therefore can be uncertain. The closed-loop dynamics of the system obtained by applying the control input (10) and expressed in port-Hamiltonian form is

$$\begin{bmatrix} \dot{q} \\ \dot{p} \end{bmatrix} = \begin{bmatrix} 0 & k_m I \\ -k_m I & -k_m D - G k_v G^T \end{bmatrix} \begin{bmatrix} \nabla_q H_d \\ \nabla_p H_d \end{bmatrix} - \begin{bmatrix} 0 \\ G\delta \end{bmatrix}, \tag{11}$$

where the total energy is $H_d = \frac{1}{2k_m} p^T M^{-1} p + \frac{k}{2k_m}\left(\sum_{i=1}^{n} q_i^2 + \frac{k_p k_m}{k}\left(\theta - \theta^*\right)^2 - \frac{\theta^2}{n}\right)$, which has a strict minimizer at the equilibrium $(\theta, \dot{\theta}) = (\theta^*, 0)$ and verifies the matching PDEs (see Section 2.1) with $M_d = k_m M$ and $J_2 = 0$, while $G^T = [1, 1, 1]$ if $n = 3$ (see [11] for details).

3.2 | Ancillary control and tube dynamics for direct-torque actuation

The ancillary control is defined here for soft continuum manipulators with direct-torque actuation by employing (5). To this end, we define a sub-domain of attraction for the closed-loop system (11), that is

$$\Omega_c = \left\{ (q, p) \in \mathbb{R}^{2n} | H_d\left(q, p\right) < c \right\}, \tag{12}$$

where c is a positive scalar time-varying parameter representing the width of the dynamic tube. Once the system trajectory enters the sub-domain of attraction (11) it should remain there indefinitely. To this end, the closed-loop energy H_d should decrease at a faster rate than the scalar c. Conversely, in case the system trajectory lies outside the sub-domain of attraction, the additional control action u_0 is introduced to bring the system trajectories to Ω_c.

Proposition 1: Consider system (1) with *Assumptions 1* and *2* in closed-loop with the IDA-PBC control law (4) where u_{es} is given in (10), while u_0 and the tube dynamics $\dot{c}$ are defined as

$$\begin{aligned} u_0 &= -\alpha c \tfrac{1}{k_m}\dot{\theta}, \\ \dot{c} &= \tfrac{1}{k_m}\left|\dot{\theta}\right|\varepsilon - \alpha c \tfrac{1}{k_m^2}\dot{\theta}^2. \end{aligned} \tag{13}$$

Assume that the parameter α verifies the condition $k_v \geq \alpha c$. Then, all system trajectories originating in Ω_c remain in Ω_c indefinitely. In addition, all system trajectories starting outside Ω_c converge to Ω_c asymptotically.

Proof: Computing the time derivative of H_d and substituting (11) yields

$$\dot{H}_d = -\left(M^{-1}p\right)^T\left(\frac{D}{k_m} + G\frac{k_v}{k_m^2}G^T\right)\left(M^{-1}p\right) - \frac{1}{k_m}\left(M^{-1}p\right)^T G\delta,$$

and substituting $\dot{\theta} = G^T M^{-1} p$ gives

$$\dot{H}_d \leq -\left(M^{-1}p\right)^T\left(\frac{D}{k_m}\right)\left(M^{-1}p\right) - \frac{k_v}{k_m^2}\dot{\theta}^2 + \frac{1}{k_m}\left|\dot{\theta}\right|\left|\delta\right|. \tag{14}$$

To prove the first claim we compute the inequality $\dot{H}_d < \dot{c}$, or equivalently $\dot{H}_d - \dot{c} < 0$, while substituting (13) and (14), which yields

$$\dot{H}_d - \dot{c} \leq -\left(M^{-1}p\right)^T\left(\frac{D}{k_m}\right)\left(M^{-1}p\right) - \frac{k_v}{k_m^2}\dot{\theta}^2 + \frac{1}{k_m}\left|\dot{\theta}\right|\left|\delta\right| - \frac{1}{k_m}\left|\dot{\theta}\right|\varepsilon + \alpha c\frac{1}{k_m^2}\dot{\theta}^2. \tag{15}$$

Since $D > 0$ and $|\delta| < \varepsilon$ by hypothesis, it follows from (15) that

$$\dot{H}_d - \dot{c} \leq -\left(M^{-1}p\right)^T\left(\frac{D}{k_m}\right)\left(M^{-1}p\right) - \frac{k_v - \alpha c}{k_m^2}\dot{\theta}^2 \leq 0.$$

which is verified for all $\alpha c \leq k_v$, thus the system trajectories starting in Ω_c remain in Ω_c indefinitely.

To prove the second claim we define the Lyapunov function candidate $W = H_d - c$ which according to (12) is positive definite outside Ω_c. Computing its time-derivative while introducing u_0 and substituting $\dot{c}$ from (13) yields

$$\dot{W} \leq -\left(M^{-1}p\right)^T\left(\frac{D}{k_m} + G\frac{k_v}{k_m^2}G^T\right)\left(M^{-1}p\right) + \frac{u_0}{k_m}\dot{\theta} + \frac{1}{k_m}\left|\dot{\theta}\right|\left(\left|\delta\right| - \varepsilon\right) + \alpha c\frac{1}{k_m^2}\dot{\theta}^2. \tag{16}$$

Substituting u_0 from (13) into (16) yields

$$\dot{W} \leq -\left(M^{-1}p\right)^T\left(\frac{D}{k_m} + G\frac{k_v}{k_m^2}G^T\right)\left(M^{-1}p\right) - \frac{1}{k_m}\left|\dot{\theta}\right|\left(\varepsilon - \left|\delta\right|\right) \leq 0,$$

where $|\delta| < \varepsilon$, thus W converges to zero and the system trajectories starting outside Ω_c converge to Ω_c asymptotically concluding the proof ■

3.3 | Dynamical model for fluidic actuation through variable flow rate

In case the soft continuum manipulator is actuated by a variable flow rate through an appropriate valve arrangement, a different system model is employed which includes the pressure dynamics of the fluid. In addition, a further assumption is introduced.

Assumption 3: The fluid is isentropic and inviscid, and the bulk modulus Γ_0, which characterizes its compressibility, is known. The pressure P of the fluid, its density ρ, and its speed v are uniform. In addition, the pressure P is known at any instant and bounded. Finally, the disturbances δ act on the system dynamics in the same way as the pressure, that is, they are matched with respect to the pressure but they are not affine in the control input.

For inextensible manipulators, the volume of the fluid in the internal chamber can be approximated as $V = V_0 + Ar\theta$, where A is the area of the cross section of the internal chamber and r is the distance from the centroid of the chamber to the center of the section, while the constant V_0 includes the volume of the supply pipes (see Figure 2). It follows that the speed of the fluid flow can be approximated as $v = r\dot{\theta}$. In case of incompressible fluids, the total mechanical energy is given by $H = \frac{1}{2}p^T M^{-1} p + \frac{1}{2}q^T K q + \Phi$, where $\Phi = \left(-P + \Gamma_0(e^{P/\Gamma_0} - 1) + \frac{1}{2}\rho r^2\dot{\theta}^2\right)(V_0 + Ar\theta)$ is the sum of the internal energy and of the kinetic energy of the fluid [20]. The system dynamics in port-Hamiltonian form is thus

$$\begin{bmatrix}\dot{q}\\ \dot{p}\\ \dot{P}\end{bmatrix} = \begin{bmatrix}0 & I & 0\\ -I & -D & \frac{\Gamma_0 Ar}{V}G\\ 0 & -\frac{\Gamma_0 Ar}{V}G^T & 0\end{bmatrix}\begin{bmatrix}\nabla_q H\\ \nabla_p H\\ \nabla_P H\end{bmatrix} + \begin{bmatrix}0\\ -G\delta\\ \frac{\Gamma_0}{V}u\end{bmatrix}, \tag{17}$$

where the system states are the position $q \in \mathbb{R}^n$, the momenta $p = \widehat{M}\dot{q}$, where $\widehat{M} = M + \rho r^2 V G G^T$ includes the inertia of the fluid, and the pressure $P \in \mathbb{R}$ in case of a single pressurized chamber. In the absence of disturbances, the control law for the regulation of the tip angle $\theta = \theta^*$ computed with an energy-shaping procedure [20] is

$$u_{\text{es}} = Ar\dot{\theta} - \frac{(V_0 + Ar\theta)}{\Gamma_0}\frac{\left(1 + k_m\left(-\frac{k}{n} + k_p k_m\right)\right)}{k_m Ar}\dot{\theta} + \frac{(V_0 + Ar\theta)}{\Gamma_0}k_i\left(\frac{k}{n}\theta + k_p k_m\left(\theta^* - \theta\right) - PAr\right), \tag{18}$$

where the tuning parameters are k_m, k_p, k_i. Note that in this case the parameter k_v is missing, since the energy-shaping procedure does not include a damping assignment. Instead, the parameter k_i refers to the internal energy of the fluid. Similarly to (10), the control law (18) depends on $\theta, \dot{\theta}$, and does not depend on the damping parameter b.

The closed-loop dynamics resulting from (18) expressed in port-Hamiltonian form is given as in [20]

$$\begin{bmatrix}\dot{q}\\ \dot{p}\\ \dot{P}\end{bmatrix} = \begin{bmatrix}0 & k_m I & 0\\ -k_m I & -k_m D & \frac{1+k_m\left(-\frac{k}{n}+k_p k_m\right)}{Ar}G\\ 0 & -\frac{1+k_m\left(-\frac{k}{n}+k_p k_m\right)}{Ar}G^T & -\frac{k_i}{Ar}\end{bmatrix}\begin{bmatrix}\nabla_q H_d\\ \nabla_p H_d\\ \nabla_P H_d\end{bmatrix} - \begin{bmatrix}0\\ G\delta\\ 0\end{bmatrix}, \tag{19}$$

where $H_d = \frac{1}{2k_m}p^T\widehat{M}^{-1}p + \frac{k}{2k_m}\left(\sum_{i=1}^n q_i^2 + \frac{k_p k_m}{k}\left(\theta - \theta^*\right)^2 - \frac{\theta^2}{n}\right) + \varsigma^2/2$, and $\varsigma = -\frac{k\theta}{n} - k_p k_m\left(\theta^* - \theta\right) + PAr$. In particular, H_d has a strict minimizer at the equilibrium $(\theta, \dot{\theta}, P) = (\theta^*, 0, P^*)$, where $P^* = \frac{k\theta^*}{nAr}$ in the absence of disturbances. Since system (17) has an extended dynamics compared to (1), the control law (18) is more complex than (10), and the closed-loop Hamiltonian also depends on the pressure P.

3.4 | Ancillary control and tube dynamics for fluidic actuation

Similarly to (12), the sub-domain of attraction for the closed-loop system (19) is defined as

$$\Omega_c = \left\{ (q, p, P) \in \mathbb{R}^{2n+1} \, | H_d \, (q, p, P) < c \right\}, \tag{20}$$

where c is the width of the dynamic tube. Note that in this case Ω_c depends also on the pressure P.

Proposition 2: Consider system (17) with *Assumptions 1* to *3* in closed-loop with the control law

$$u_{\text{ida-pbc}} = \begin{cases} u_{\text{es}} & H_d \, (q, p, P) < c, \\ u_{\text{es}} + u_0 & H_d \, (q, p, P) \geq c, \end{cases} \tag{21}$$

where u_{es} is given in (18), while u_0 and $\dot{c}$ are defined as

$$\begin{aligned} u_0 &= -\alpha c \varsigma \tfrac{V}{\Gamma_0 A r}, \\ \dot{c} &= \tfrac{1}{k_m} \left| \dot{\theta} \right| \varepsilon - \alpha c \varsigma^2. \end{aligned} \tag{22}$$

Assume that the parameter α verifies the condition $k_i A r \geq \alpha c$. Then, all system trajectories originating in Ω_c remain in Ω_c indefinitely. In addition, all system trajectories starting outside Ω_c converge to Ω_c asymptotically.

Proof: Computing the time derivative of H_d and substituting (19) yields

$$\dot{H}_d = -\left(\widehat{M}^{-1} p \right)^T \left(\frac{D}{k_m} \right) \left(\widehat{M}^{-1} p \right) - \frac{1}{k_m} \left(\widehat{M}^{-1} p \right)^T G \delta - k_i A r \varsigma^2.$$

and thus

$$\dot{H}_d \leq -\left(\widehat{M}^{-1} p \right)^T \left(\frac{D}{k_m} \right) \left(\widehat{M}^{-1} p \right) - k_i A r \varsigma^2 + \frac{1}{k_m} \left| \dot{\theta} \right| |\delta| \, . \tag{23}$$

To prove the first claim we compute the inequality $\dot{H}_d < \dot{c}$, or equivalently $\dot{H}_d - \dot{c} < 0$, while substituting (22) and (23), which yields

$$\dot{H}_d - \dot{c} \leq -\left(\widehat{M}^{-1} p \right)^T \left(\frac{D}{k_m} \right) \left(\widehat{M}^{-1} p \right) - k_i A r \varsigma^2 + \frac{1}{k_m} \left| \dot{\theta} \right| |\delta| - \frac{1}{k_m} \left| \dot{\theta} \right| \varepsilon + \alpha c \varsigma^2. \tag{24}$$

Since $D > 0$ and $|\delta| < \varepsilon$ by hypothesis (see *Assumption 2*), it follows from (24) that

$$\dot{H}_d - \dot{c} \leq -\left(\widehat{M}^{-1} p \right)^T \left(\frac{D}{k_m} \right) \left(\widehat{M}^{-1} p \right) - (k_i A r - \alpha c) \varsigma^2 \leq 0,$$

which is verified for all $\alpha c \leq k_i A r$. Thus, the trajectories of the closed-loop system starting in Ω_c will remain in Ω_c indefinitely.

To prove the second claim we define the Lyapunov function candidate $W = H_d - c$ similarly to (16). Computing its time-derivative while introducing u_0 and substituting $\dot{c}$ from (22) yields

$$\dot{W} \leq -\left(\widehat{M}^{-1} p \right)^T \left(\frac{D}{k_m} \right) \left(\widehat{M}^{-1} p \right) - k_i A r \varsigma^2 + u_0 \frac{\Gamma_0 A r}{V} \varsigma + \frac{1}{k_m} \left| \dot{\theta} \right| (|\delta| - \varepsilon) + \alpha c \varsigma^2. \tag{25}$$

Substituting u_0 from (22) into (25) yields

$$\dot{W} \leq -\left(\widehat{M}^{-1}p\right)^T \left(\frac{D}{k_m}\right)\left(\widehat{M}^{-1}p\right) - k_i A r \varsigma^2 + \frac{1}{k_m}\left|\dot{\theta}\right|(|\delta| - \varepsilon) \leq 0,$$

thus W converges to zero and the system trajectories starting outside Ω_c converge to Ω_c asymptotically ■

Remark 1. Differently from (5) which requires full state feedback, (13) only depends on the output $\dot{\theta}$. Inspecting (13) shows that the term u_0 modifies the damping assignment, which is governed by the parameter k_v, by introducing a further damping term proportional to the tube width c. Instead, the control u_0 in (22) introduces a term proportional to ς which contains the position error $(\theta^* - \theta)$ but does not depend on the velocity $\dot{\theta}$. Thus u_0 in (22) increases the parameter k_i by the amount αc yielding a stronger proportional-control action. Inspecting (19) however, reveals that k_i is also associated to dissipation, but this effect is related to the pressure dynamics rather than to the velocity. In conclusion, the term u_0 is associated to dissipation for both system models, which results from employing energy-shaping principles based on IDA-PBC. However, the type of dissipation depends on the specific model and does not necessarily correspond to damping.

Remark 2. It follows from *Assumptions 2* and *3* that only the effect of matched disturbances is considered in either (13) or (22). In principle, unmatched disturbances could be accounted for by including an adaptive observer (see Proposition 2 in [37]). However, the limitations imposed by *Assumption 1* (i.e. that only θ and its time derivative are directly measurable) precludes this possibility. To highlight this point we rewrite (15) for the case of matched and unmatched disturbances, which yields after factoring common terms

$$\dot{H}_d - \dot{c} \leq -\left(M^{-1}p\right)^T \left(\frac{D}{k_m}\right)\left(M^{-1}p\right) - \frac{k_v - \alpha c}{k_m^2}\dot{\theta}^2 + \frac{1}{k_m}\left(\left|M^{-1}p\right||\delta| - \left|\dot{\theta}\right|\varepsilon\right).$$

Note that the inequality $\left|M^{-1}p\right||\delta| - \left|\dot{\theta}\right|\varepsilon < 0$ resulting from the last term is not verified for any ε in case $\dot{\theta} = 0$ and $\left|M^{-1}p\right| \neq 0$. This condition can occur if the angular velocities of different virtual joints have opposite sign, that is $\dot{q}_i\dot{q}_j < 0$ for some i, j. In addition, defining the tube dynamics as $\dot{c} = \frac{1}{k_m}\left|M^{-1}p\right|\varepsilon - \alpha c\frac{1}{k_m^2}\dot{\theta}^2$ yields a non-implementable expression, in case the position q and the velocity $\dot{q}$ of the virtual joints which appear in $M^{-1}p$ are not measurable. This limitation might be overcome by estimating q and $\dot{q}$ with a state observer, which shall be investigated in future work. Conversely, if $\dot{q}_i\dot{q}_j > 0$, there exist some ε such that $|M^{-1}p||\delta| < |\dot{\theta}|\varepsilon$, which suggests that the ancillary control laws (13) and (22) actually have some ability to reject unmatched disturbances (see Section 4).

4 | SIMULATION RESULTS

This section illustrates the proposed dynamic tube-MPC for a soft continuum manipulator, which is an underactuated mechanical system. Both direct-torque actuation through a regulated pressure and fluidic actuation through a variable flow rate are considered. The system is subject to parametric uncertainty and external disturbances, either constant and matched or time-varying and unmatched.

Simulations have been conducted for a model with $n = 3$ DOFs and $m = 1$ control input, resulting in an underactuation degree $n - m = 2$. This choice is motivated by our experimental work (see [5, 11]) which has demonstrated that this approximation is appropriate for our soft continuum manipulator prototypes. Note however, that the control laws (10), (13) and (18), (22) are valid for any value of n. The position vector is $q = (q_1, q_2, q_3)^T$, and the initial configuration corresponds to all links aligned, that is $q(t_0) = (0, 0, 0)^T$. The system output is $y = G^T q = q_1 + q_2 + q_3 = \theta$. The time discretization has been implemented with 150 points, the initial time is $t_0 = 0.0s$, the final time is $t_f = 5.0$ s, thus the

time interval is $t_f - t_0 = 5.0$ s, and the time step is $dt = 0.0336$ s. The tuning parameters in (10) have been chosen empirically as $k_p = 0.1$, $k_v = 0.6$, $k_m = 22.0$, and $\varepsilon = 1.0$ in (13). The weights in the performance index of the nonlinear programming problem have been tuned empirically as $\beta_{\text{obj}} = 0.1$ and $\gamma_{\text{obj}} = 1.0$.

4.1 | Direct-torque actuation through regulated pressure

The equations of motion for the model with direct-torque actuation through regulated pressure is

$$M(q)\ddot{q} + D\dot{q} + Kq = Gu \tag{26}$$

where M, D, K, G are defined in the Appendix. The dynamic tube-MPC problem $\mathcal{P}$ is defined by the constraints and equations in Table 1: the residual equation of motion corresponding to the constraint $\mathbf{c}_{\text{mot}}$; the dynamic tube constraint $\mathbf{c}_{\text{tube}}$; the IDA-PBC control law used in the auxiliary constraint $\mathbf{c}_{\text{aux}}$, where k_p, k_v, and k_m are tuning parameters (see Section 3.1). Note that P and $\dot{P}$ are not included in the design variables in this case. To assess the effectiveness of the proposed algorithm, model uncertainties and bounded external disturbances have been considered in addition to the inherent numerical optimization errors. In particular, the model uncertainties are related to the damping b in the virtual joints, such that the difference between model and plant is $\Delta b = 0.0001$ Ns/rad, while the external matched disturbances are $\boldsymbol{\delta} = \delta_0 \times [1; 1; 1]$ Nm with $\delta_0 > 0$ corresponding to a bending moment applied to the distal link.

Figure 3 shows the simulation results for an output trajectory corresponding to an hyperbolic tangent, that is $y_d(t) = \frac{\pi}{12}(1 + \tanh(\frac{5}{2}(t - 2.5)))$. In this case, we have set $k_b = 800$, $k_a = 1$, and $\rho_\infty = 0.5$, while the output error tolerance is 0.0195 rad. Figure 3(a) shows the reference trajectory and Figure 3(b) shows that the control policy corrects the output during the time interval $2.4 \leq t \leq 2.6$. Figure 3(c) shows the output error $y_d - y$, which has a maximum amplitude of approximately 0.023 rad. Figure 3(d) shows the angular positions of the virtual joints, which are almost coincident, Figure 3(e) shows the corresponding angular velocities, and Figure 3(f) shows the phase diagram. Figure 3(g) and Figure 3(h) show the time history of the tube variable α and of its time derivative $\dot{\alpha}$, which is not constant differently from our previous implementation [37]. Figure 3(i) shows the tube geometry that is updated when the dynamic tube-MPC is activated. The parameter c decrease exponentially when the output error falls below the predefined tolerance and u_{fb} is deactivated. In summary, oscillations in the tube variables (α, $\dot{\alpha}$) and in the tube geometry (c) are indicative of the complexity of the tracking problem. The sudden variation of the tube variables results in a corresponding change of the control policy which has the effect of reducing the output error. Thus, a suitable choice of the tuning parameters for the specific tracking problem is essential for good tracking performance. In this

Constraints	Equation/function	Soft manipulator with direct-torque actuation
$\mathbf{c}_{\text{mot}}$	$\mathbf{res}(q, \dot{q}, \ddot{q}, u)$	$M(q)\ddot{q} + D\dot{q} + Kq - Gu$
$\mathbf{c}_{\text{tube}}$	$w_1(q, \dot{q})$; $w_2(q, \dot{q})$	$w_1(q, \dot{q}) = \frac{1}{k_m}\lvert\dot{\theta}\rvert$; $\quad w_2(q, \dot{q}) = \frac{1}{k_m^2}\dot{\theta}^2$
$\mathbf{c}_{\text{aux}}$	$u_{\text{es}}(q, \dot{q})$	$u_{\text{es}} = \frac{k}{n}\theta + k_p k_m(\theta^* - \theta) - \frac{k_v}{k_m}\dot{\theta}$
	$u_0(q, \dot{q})$	$-\alpha c \frac{1}{k_m}\dot{\theta}$
	$H_d(q, \dot{q})$	$\frac{1}{2k_m}p^T M^{-1} p + \frac{k}{2k_m}\left(\sum_{i=1}^{n} q_i^2 + \frac{k_p k_m}{k}(\theta - \theta^*)^2 - \frac{\theta^2}{n}\right)$

TABLE 1 Constraints and functions related to the optimization problem $\mathcal{P}$ for direct-torque actuation.

respect, higher complexity due to the system dynamics or to the specific trajectory can pose numerical challenges.

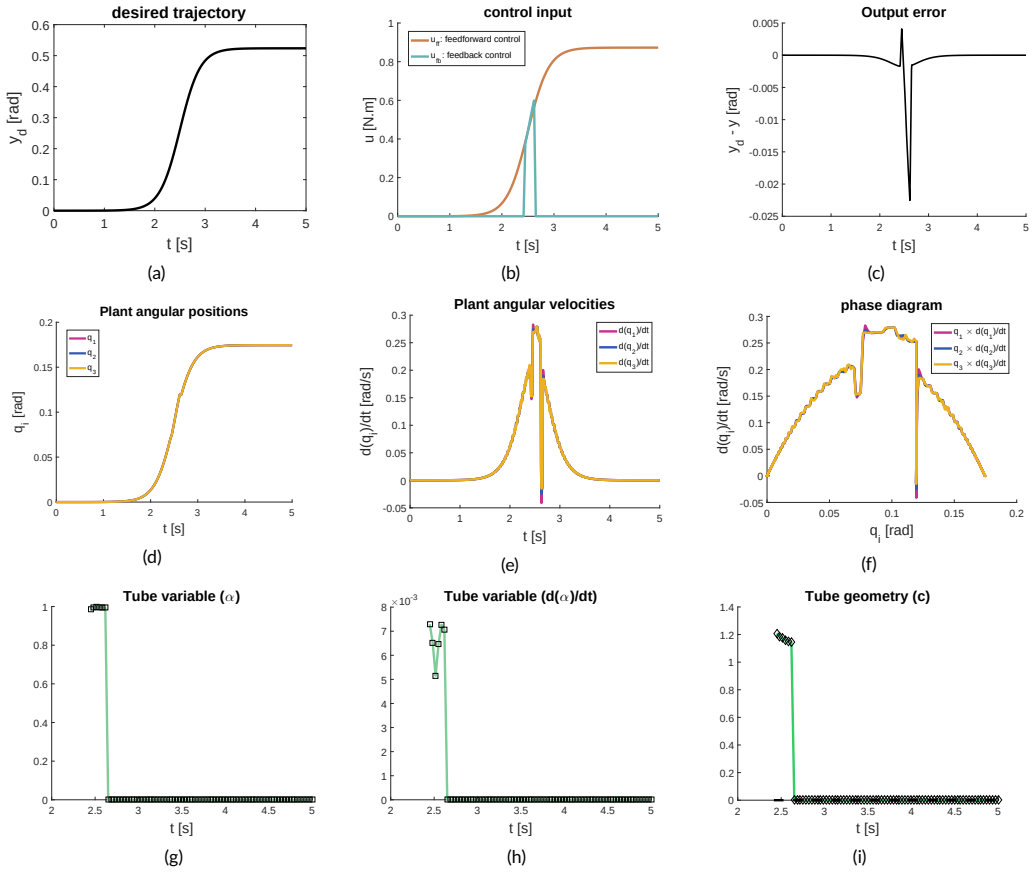


FIGURE 3 Simulation results for direct-torque actuation ($\rho_\infty = 0.5$).

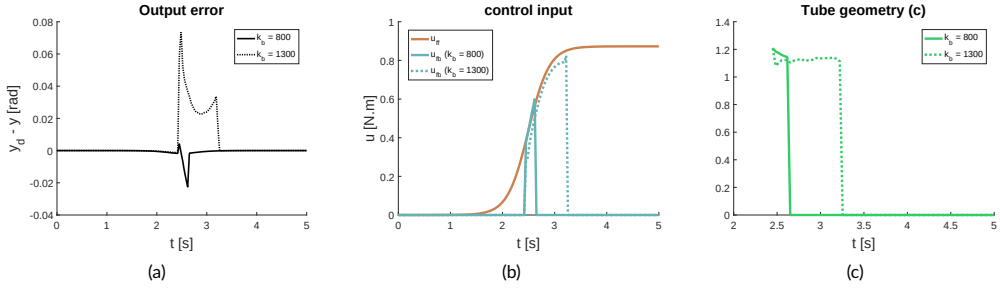


FIGURE 4 Simulation results illustrating the effect on performance of the parameter k_b in (5).

Figure 4 illustrates the effect on performance of the parameter k_b in (5) considering the values $k_b = 1300, 800$. In

this case/problem, convergence is achieved by $330 \leq k_b \leq 1300$. Note that the values of k_b and k_a are specific to the model parameters and to the target trajectory. The effect of different matched disturbances has been assessed using $\delta = 0.00001 \times [1; 1; 1]$ as reference and three multiplicative factors (i.e, factor $= 1, 200, 1000$) with the same tuning parameters. The system response is illustrated in Figure 5: while the simulation results indicate that the dynamic tube-MPC can cope with different disturbances, a constant output error is nevertheless present. In particular, the error is smaller for the reference representing the smallest disturbance since the controller parameters have been tuned for this condition, which corresponds to Figure 3. Note that further performance improvements can be obtained for the larger disturbances (i.e., factor= 200 and 1000) by appropriately tuning the control policy gains. A further set of results is shown in Figure 6 in order to compare the dynamic tube-MPC with a simpler tube-MPC that employs fixed values of α and c, as in [29]. The results indicate that the proposed dynamic tube-MPC yields a smaller output error and a reduced control action.

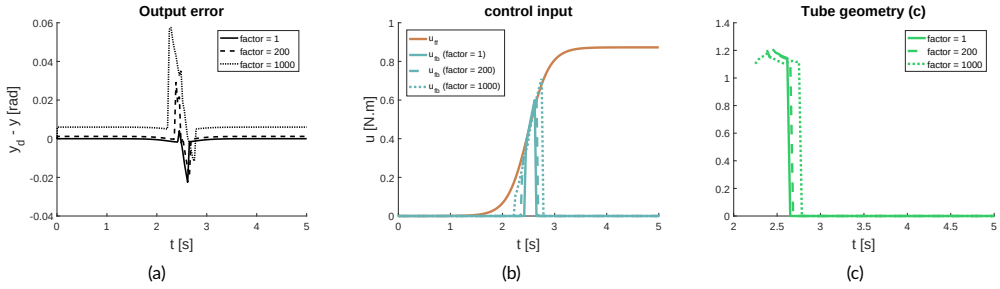


FIGURE 5 Simulation results illustrating the sensitivity to external disturbance.

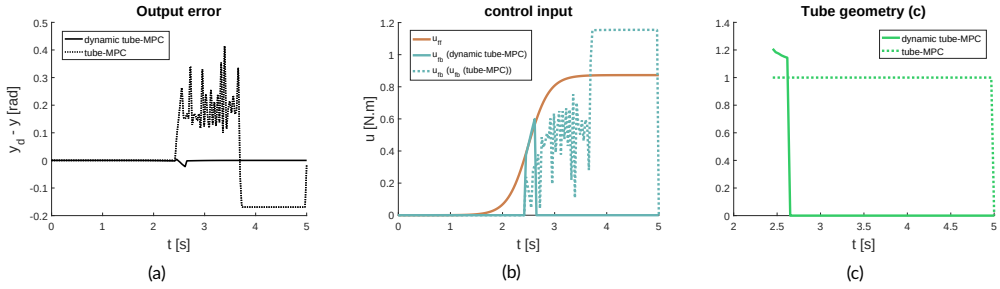


FIGURE 6 Simulation results comparing the proposed dynamic tube-MPC with a tube-MPC that has fixed tube parameters.

4.2 | Fluidic actuation through variable flow rate

For the soft manipulator with fluidic actuation achieved through a variable flow rate (see Section 3.3), the equations of motion employed in the MPC optimization problem also include the pressure dynamics, that is

$$\begin{aligned} \widehat{M}(q)\ddot{q} + D\dot{q} + Kq - GP = 0 \\ (V_0 + Ar(G^T q))\dot{P}/\Gamma_0 + Ar(G^T \dot{q}) = u, \end{aligned} \tag{27}$$

where $u[mm^3/s]$ is the volumetric flow rate, $\dot{P}$ is the time derivative of the pressure P, and $\widehat{M}(q)$ has been defined previously (see Section 3.3). The model parameters in (27) have been chosen for illustrative purposes as $A = 28.27$ mm^2, $V_0 = 24.74$ mm^3, $r = 3 \times 10^{-3}$ m, and $\Gamma_0 = 2 \times 10^4$ bar, $\rho = 1$ g/cm^3 corresponding to water. The constraints and the functions that define the MPC optimization problem $\mathcal{P}$ are given in Table 2. Note that P and $\dot{P}$ are included in the design variables in this case.

Constraints	Equation/function	Soft manipulator with fow-rate actuation
$\mathbf{c}_{\text{mot}}$	$\mathbf{res}(q, \dot{q}, \ddot{q}, P, \dot{P}, u)$	$\begin{pmatrix} \widehat{M}(q)\ddot{q} + D\dot{q} + Kq - GP \\ (V_0 + Ar(G^T q))\dot{P}/\Gamma_0 + Ar(G^T \dot{q}) - u \end{pmatrix}$
$\mathbf{c}_{\text{tube}}$	$w_1(q, \dot{q})$; $w_2(q, \dot{q}, P)$	$w_1(q, \dot{q}) = \frac{1}{k_m}\lvert\dot{\theta}\rvert$; $\quad w_2(q, \dot{q}) = \varsigma^2$
$\mathbf{c}_{\text{aux}}$	$u_{\text{es}}(q, \dot{q})$	$Ar\dot{\theta} - \frac{(V_0+Ar\theta)}{\Gamma_0}\frac{\left(1+k_m\left(-\frac{k}{n}+k_p k_m\right)\right)}{k_m Ar}\dot{\theta} + \frac{(V_0+Ar\theta)}{\Gamma_0}k_i\left(\frac{k}{n}\theta + k_p k_m(\theta^* - \theta) - PAr\right)$
	$u_0(q, \dot{q})$	$-\alpha c\varsigma\frac{V}{\Gamma_0 Ar}$
	$H_d(q, \dot{q})$	$\frac{1}{2k_m}p^T\widehat{M}^{-1}p + \frac{k}{2k_m}\left(\sum_{i=1}^{n} q_i^2 + \frac{k_p k_m}{k}(\theta - \theta^*)^2 - \frac{\theta^2}{n}\right) + \varsigma^2/2$

TABLE 2 Constraints and functions defining the optimization problem $\mathcal{P}$ for fluidic actuation through a variable flow-rate.

Figure 7 considers an output trajectory corresponding to an hyperbolic secant, that is $y_d(t) = \frac{\pi}{24}\text{sech}(\frac{7}{3}(t-2.5))$, and shows the effect of the time-varying unmatched disturbances $\delta = 0.001 \times [\sin(4t); \sin(4t + \pi/10); \sin(4t + \pi/8)]$, where the phase shifts $\pi/10$ and $\pi/8$ are related to the second and third virtual joint, in addition to the uncertain damping. The same tuning parameters have been employed as in Figure 3, while the control policy gains have been set to $k_b = -3.0$ and $k_a = 0.06$ and a different reference trajectory has been used. In summary, the feedforward control is different due to the new trajectory, and the tube geometry is more complex due to the pressure dynamics of the fluid, and the time-varying unmatched disturbances considered.

A further set of results is shown in Figure 8 in order to compare the proposed dynamic tube-MPC implementation (i.e. v2), which accounts for the fact that both α and $\dot{\alpha}$ are time-varying in the modified equality constraints $\mathbf{c}_\alpha$ of $\mathcal{P}$, with our previous work [37] (i.e. denoted by v1) in the presence of a more complex dynamics, a different trajectory, and time-varying external disturbances. The results show that the proposed dynamic tube-MPC yields a smaller tracking error compared to [37] (i.e. the output error for v2 goes to zero in Figure 8(a)) thanks to a more complex tube geometry (see Figure 8(c)). In addition, Figure 8(d)) to Figure 8(f)) correspond to smaller values of the gains k_a and k_b in (9) (i.e. the values are 40% smaller compared to Figure 8(a)). In this respect, the results indicate that the proposed dynamic tube-MPC implementation is less sensitive to the tuning parameters and yields a more consistent response, which can be beneficial in engineering practice. Figure 9 shows a set of simulation results related to a non-smooth trajectory,

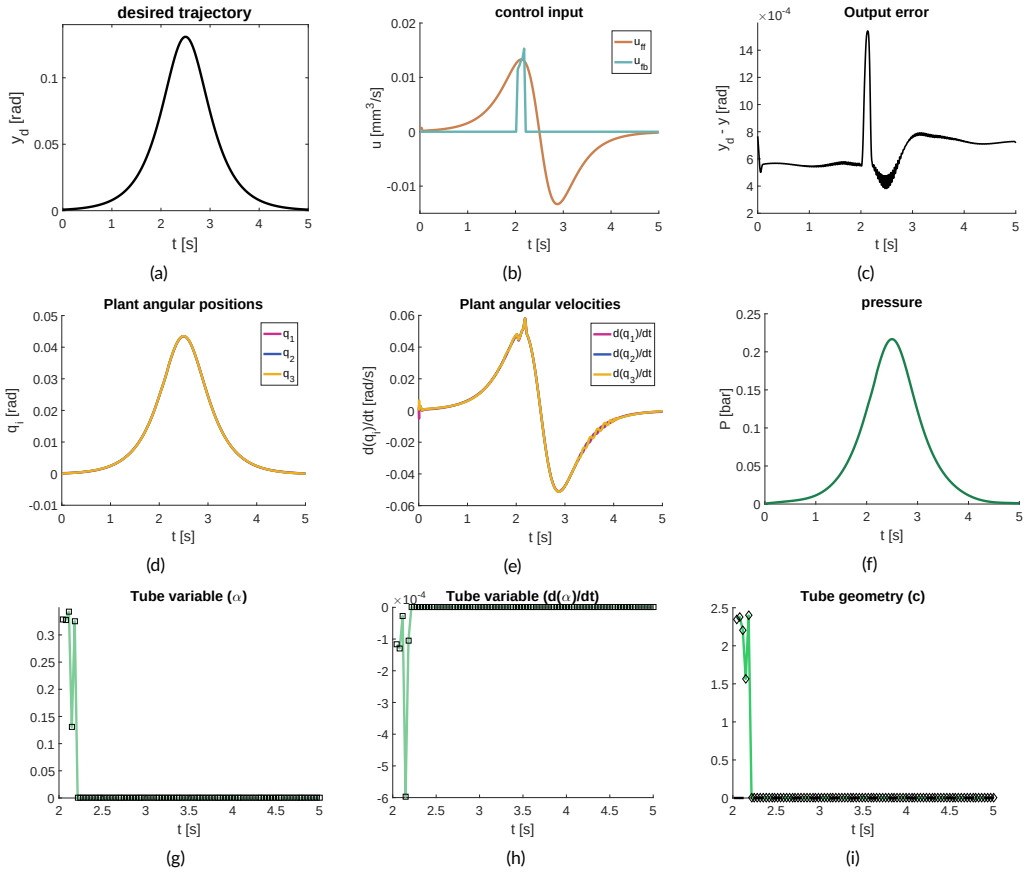


FIGURE 7 Simulation results for the case of fluidic actuation with $\rho_\infty = 0.5$ and unmatched disturbances.

where six intermediate points were taken from the reference trajectory in Figure 7 and were connected with a linear interpolation method. The control policy gains were tuned as $k_b = -10$ and $k_a = 0.2$. The results highlight the ability of the proposed algorithm to deal with non-smooth trajectories for the class of soft continuum manipulators considered in this work. Additional results for the tracking control of different underactuated mechanisms with non-smooth trajectories have been presented in our previous work [37]

5 | CONCLUSION

This work presented a dynamic tube-Model Predictive Control formulation for the tracking control of soft continuum planar inextensible manipulators with fluidic actuation. In particular, the ancillary control was derived analytically with energy-shaping principles, and it introduces a dissipative action when the trajectories are outside the sub-domain of attraction corresponding to the dynamic tube. Simulations results indicate that the proposed control policy yields satisfactory tracking performance in the presence of either time-varying or constant bounded disturbances, and it performs better than a fixed tube-Model Predictive Control yielding smaller output errors across different types of

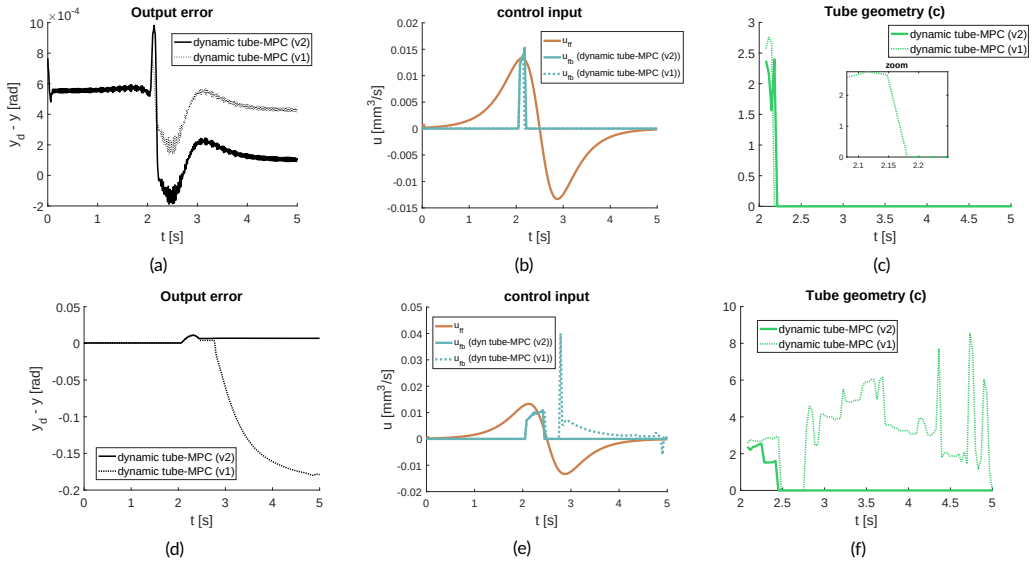


FIGURE 8 Simulation results comparing the proposed dynamic tube-MPC (i.e. v2) with our previous implementation [37] (i.e. v1). Figure 8(a)-8(c) employ the same tuning parameters of Figure 7. Figure 8(d)-8(f) employ 40% smaller values of k_a and k_b for both v1 and v2.

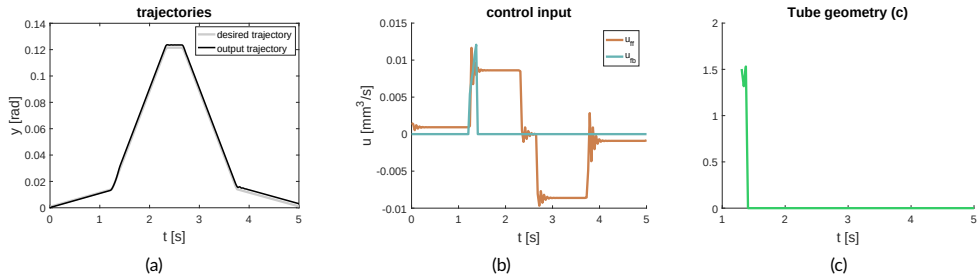


FIGURE 9 Simulation results for a non-smooth trajectory.

disturbances, and exhibiting lower sensitivity to the tuning parameters, which is beneficial in engineering practice.

Nevertheless, a number of aspects require further investigation. First of all, the ancillary control and the tube dynamics have been designed assuming that the disturbances are matched. In principle, this assumption could be relaxed by estimating the position and the velocity of the virtual joints with a state observer at the cost of higher complexity of the control algorithm. Furthermore, the proposed models do not account explicitly for the effect of gravity, even though this can be included in the lumped disturbance. In principle, including the effect of gravity within the potential energy of the system is expected to yield faster response and better tracking performance, thus it shall be investigated in future work. The class of systems considered in this work shall be extended to include different types of soft continuum robots and different actuation strategies. Finally, we aim to study the effect of the tuning parameters on performance and on stability, to investigate the stability of the proposed algorithm, and to conduct experimental tests with our prototypes.

CONFLICT OF INTEREST

The authors declare that they have no conflict of interest to this work.

DATA AVAILABILITY STATEMENT

The data that support the findings of this study is available from the corresponding author upon reasonable request.

ORCID

Guaraci Bastos Jr. https://orcid.org/0000-0002-8174-4102
Enrico Franco https://orcid.org/0000-0001-9991-7377

REFERENCES

[1] Suzumori K, Iikura S, Tanaka H. Development of flexible microactuator and its applications to robotic mechanisms. In: Proceedings. 1991 IEEE International Conference on Robotics and Automation IEEE Comput. Soc. Press; 1991. p. 1622–1627.

[2] Garriga-Casanovas A, Collison I, Rodriguez y Baena F. Toward a Common Framework for the Design of Soft Robotic Manipulators with Fluidic Actuation. Soft Robotics 2018 8;5(5):622–649.

[3] Suzumori K, Miyagawa T, Kimura M, Hasegawa Y. Micro inspection robot for 1-in pipes. IEEE/ASME Transactions on Mechatronics 1999;4(3):286–292.

[4] Gerboni G, Ranzani T, Diodato A, Ciuti G, Cianchetti M, Menciassi A. Modular soft mechatronic manipulator for minimally invasive surgery (MIS): overall architecture and development of a fully integrated soft module. Meccanica 2015 9;50(11):2865–2878.

[5] Franco E, Garriga-Casanovas A, Tang J, Rodriguez y Baena F, Astolfi A. Adaptive energy shaping control of a class of nonlinear soft continuum manipulators. IEEE ASME Trans Mechatron 2021;p. 1–11.

[6] Best CM, Rupert L, Killpack MD. Comparing model-based control methods for simultaneous stiffness and position control of inflatable soft robots. The International Journal of Robotics Research 2020 5;40(1):470–493.

[7] Liu Z, Cai Z, Peng H, Zhang X, Wu Z. Morphology and Tension Perception of Cable-Driven Continuum Robots. IEEE/ASME Transactions on Mechatronics 2022;.

[8] Zhang J, Hu Y, Li Y, Ma K, Wei Y, Yang J, et al. Versatile Like a Seahorse Tail: A Bio-Inspired Programmable Continuum Robot For Conformal Grasping. Advanced Intelligent Systems 2022 oct;p. 2200263. https://onlinelibrary.wiley.com/doi/10.1002/aisy.202200263.

[9] Zhang J, Kan Z, Li Y, Wu Z, Wu J, Peng H. Novel Design of a Cable-Driven Continuum Robot with Multiple Motion Patterns. IEEE Robotics and Automation Letters 2022 jul;7(3):6163–6170.

[10] Yang J, Peng H, Zhou W, Zhang J, Wu Z. A modular approach for dynamic modeling of multisegment continuum robots. Mechanism and Machine Theory 2021 nov;165:104429.

[11] Franco E, Garriga-Casanovas A. Energy-shaping control of soft continuum manipulators with in-plane disturbances. Int J Rob Res 2021;40(1):236–255.

[12] Falkenhahn V, Hildebrandt A, Neumann R, Sawodny O. Dynamic Control of the Bionic Handling Assistant. IEEE/ASME Transactions on Mechatronics 2017 2;22(1):6–17.

[13] Bu N, Liu H, Li W. Robust passive tracking control for an uncertain soft actuator using robust right coprime factorization. International Journal of Robust and Nonlinear Control 2021 6;31(14):6810–6825.

[14] Della Santina C, Bianchi M, Grioli G, Angelini F, Catalano M, Garabini M, et al. Controlling Soft Robots: Balancing Feedback and Feedforward Elements. IEEE Robotics and Automation Magazine 2017 9;24(3):75–83.

[15] Mattioni A, Wu Y, Ramirez H, Le Gorrec Y, Macchelli A. Modelling and control of an IPMC actuated flexible structure: A lumped port Hamiltonian approach. Control Engineering Practice 2020 8;101:104498.

[16] Ortega R, Spong MW, Gomez-Estern F, Blankenstein G. Stabilization of a class of underactuated mechanical systems via interconnection and damping assignment. IEEE Trans Autom Control 2002;47(8):1218–1233.

[17] Trumic M, Santina CD, Jovanovic K, Fagiolini A. Adaptive Control of Soft Robots Based on an Enhanced 3D Augmented Rigid Robot Matching. IEEE Control Systems Letters 2021;5(6):1934 – 1939.

[18] Franco E, Garriga Casanovas A, Donaire A. Energy shaping control with integral action for soft continuum manipulators. Mech Mach Theory 2021;158:104250.

[19] Stolzle M, Santina CD. Piston-Driven Pneumatically-Actuated Soft Robots: modeling and backstepping control. IEEE Control Systems Letters 2021;p. 1–1.

[20] Franco E. Energy Shaping Control of Hydraulic Soft Continuum Planar Manipulators. IEEE Control Systems Letters 2022;6:1748–1753.

[21] Franco E, Ayatullah T, Sugiharto A, Garriga-Casanovas A, Virdyawan V. Nonlinear energy-based control of soft continuum pneumatic manipulators. Nonlinear Dynamics 2021 9;106(1):229–253.

[22] Yaghmaei A, Yazdanpanah MJ. Trajectory tracking for a class of contractive port Hamiltonian systems. Automatica 2017 9;83:331–336.

[23] Chai R, Niu H, Carrasco J, Arvin F, Yin H, Lennox B. Design and Experimental Validation of Deep Reinforcement Learning-Based Fast Trajectory Planning and Control for Mobile Robot in Unknown Environment. IEEE Transactions on Neural Networks and Learning Systems 2022;.

[24] Allgower F, Findeisen R, Nagy ZK. Nonlinear Model Predictive Control: From Theory to Application. J Chin Inst Chem Engrs 2004;35(3):299–315.

[25] Chen H, Allgower F. A Quasi-Infinite Horizon Nonlinear Model Predictive Control Scheme with Guaranteed Stability. Automatica 1998;34(10):1205–1217.

[26] Grune L, Pannek J. Nonlinear Model Predictive Control: Theory and Algorithms. Springer-Verlag; 2017.

[27] Mayne DQ, Rawlings JB, Rao CV, Scokaert POM. Constrainerd Model Predictive Control: Stability and Control. Automatica 2000;36:789–814.

[28] Chai R, Tsourdos A, Gao H, Chai S, Xia Y. Attitude tracking control for reentry vehicles using centralised robust model predictive control. Automatica 2022 nov;145:110561.

[29] Mayne DQ, Kerrigan EC, van Wyk EJ, Falugi P. Tube-based robust nonlinear model predictive control. Int J Robust Nonlin Control 2011;21(11):1341–1353.

[30] Nikou A, Dimarogonas DV. Decentralized tube-based model predictive control of uncertain nonlinear multiagent systems. Int J Robust Nonlin Control 2019;29(10):2799–2818.

[31] Sebghati A, Shamaghdari S. Tube-based robust economic model predictive control with practical and relaxed stability guarantees and its application to smart grid. Int J Robust Nonlin Control 2020;30(17):7533–7559.

[32] Prado ÁJ, Torres-Torriti M, Yuz J, Auat Cheein F. Tube-based nonlinear model predictive control for autonomous skid-steer mobile robots with tire–terrain interactions. Control Engineering Practice 2020;101:104451.

[33] Subramanian S, Lucia S, Paulen R, Engell S. Tube-enhanced multi-stage model predictive control for flexible robust control of constrained linear systems with additive and parametric uncertainties. International Journal of Robust and Nonlinear Control 2021 6;31(9):4458–4487.

[34] El-Ferik S. RMPC for Uncertain Nonlinear Systems With Non-Additive Dynamic Disturbances and Noisy Measurements. IEEE Access 2020;8:44846–44857.

[35] Chai R, Tsourdos A, Gao H, Xia Y, Chai S. Dual-Loop Tube-Based Robust Model Predictive Attitude Tracking Control for Spacecraft with System Constraints and Additive Disturbances. IEEE Transactions on Industrial Electronics 2022 apr;69(4):4022–4033.

[36] Lopez BT, Howl JP, Slotine JJE. Dynamic tube MPC for nonlinear systems. In: Proceedings of the American Control Conference, vol. 2019-July Institute of Electrical and Electronics Engineers Inc.; 2019. p. 1655–1662.

[37] Bastos G, Franco E. Energy shaping dynamic tube-MPC for underactuated mechanical systems. Nonlinear Dynamics 2021;106:359–380.

[38] Bastos G, Seifried R, Brüls O. Analysis of stable model inversion methods for constrained underactuated mechanical systems. Mech Mach Theory 2017;111:99–117.

[39] Bastos G, Brüls O. Analysis of open-loop control design and parallel computation for underactuated manipulators. Acta Mech 2020;231:2439–2456.

[40] Chung J, Hulbert GM. A Time Integration Algorithm for Structural Dynamics with Improved Numerical Dissipation: The Generalized-α Method. ASME J Appl Mech 1993;60:371–375.

[41] Arnold M, Brüls O. Convergence of the generalized-α scheme for constrained mechanical systems. Multibody Syst Dyn 2007;18(2):185–202.

[42] Newmark NM. A method of computation for structural dynamics. J Eng Mech 1959;85:67–94.

[43] Godage IS, Wirz R, Walker ID, Webster RJ. Accurate and Efficient Dynamics for Variable-Length Continuum Arms: A Center of Gravity Approach. Soft Robotics 2015 sep;2(3):96–106.

[44] Yu YQ, Howell LL, Lusk C, Yue Y, He MG. Dynamic Modeling of Compliant Mechanisms Based on the Pseudo-Rigid-Body Model. Journal of Mechanical Design 2005 jul;127(4):760. http://mechanicaldesign.asmedigitalcollection.asme.org/article.aspx?articleid=1448594https://doi.org/10.1115/1.1900750.

APPENDIX

The matrices in equation (26) are

$$M(q) = \begin{pmatrix} c_1 + c_2\cos(q_2) + c_3\cos(q_3) + c_4\cos(q_2+q_3) & * & * \\ c_8 + c_9\cos(q_2) + c_{10}\cos(q_3) + c_{11}\cos(q_2+q_3) & c_5 + c_6\cos(q_3) & * \\ c_{12} + c_{13}\cos(q_3) + c_{14}\cos(q_2+q_3) & c_{15} + c_{16}\cos(q_3) & c_7 \end{pmatrix},$$
$$D = \begin{pmatrix} b & 0 & 0 \\ 0 & b & 0 \\ 0 & 0 & b \end{pmatrix}, K = \begin{pmatrix} k & 0 & 0 \\ 0 & k & 0 \\ 0 & 0 & k \end{pmatrix}, G = \begin{pmatrix} 1 \\ 1 \\ 1 \end{pmatrix}, \tag{A1}$$

and the constant parameters in the inertia matrix are

$$\begin{aligned} c_1 = l_1^2 m_1/4 + l_1^2 m_2 + l_1^2 m_3 + c_5, \;\; c_2 = l_1 l_2 m_2 + 2 l_1 l_2 m_3, \\ c_3 = l_2 l_3 m_3, \;\; c_4 = l_3 l_1 m_3, \;\; c_5 = l_2^2 m_2/4 + l_2^2 m_3 + c_7, \\ c_6 = c_3, \;\; c_7 = l_3^2 m_3/4, \;\; c_8 = c_5, \;\; c_9 = c_2/2, \;\; c_{10} = c_6, \\ c_{11} = c_4/2, \;\; c_{12} = c_7, \;\; c_{13} = c_3/2, \;\; c_{14} = c_4/2, \\ c_{15} = c_7, \;\; c_{16} = c_3/2. \end{aligned} \tag{A2}$$

The numerical values of the parameters are given in Table 3, where the total length of the manipulator is $l_0 = l_1+l_2+l_3+l_4$ and its total mass is $m_0 = m_1 + m_2 + m_3 + m_4$. In particular, the first link l_1 is static [11].

Parameter	Value
total length: l_0	l_0 = 100/1000 m
length: l_1	$l_0$12.5/100 m
length: l_2	$l_0$37.5/100 m
length: l_3	$l_0$37.5/100 m
length: l_4	$l_0$12.5/100 m
total mass: m_0	m_0 = 1.5/1000 kg
mass: m_1	$m_0$12.5/100 kg
mass: m_2	$m_0$37.5/100 kg
mass: m_3	$m_0$37.5/100 kg
mass: m_4	$m_0$12.5/100 kg
spring: k	5.0 N/rad
damper: b	0.015 N.s/rad

TABLE 3 Parameters of the rigid-link model (see model schematics in Figure 2)